01 Aug 2022

Temporal LiDAR Scanning in Quantifying Cumulative Rockfall Volume and Hazard Assessment: A Case Study at Southwestern Saudi Arabia

Abdullah A. Alotaibi

Norbert H. Maerz
Missouri University of Science and Technology, norbert@mst.edu

Kenneth J. Boyko

Ahmed M. Youssef

et. al. For a complete list of authors, see https://scholarsmine.mst.edu/geosci_geo_peteng_facwork/1992

Recommended Citation

A. A. Alotaibi et al., "Temporal LiDAR Scanning in Quantifying Cumulative Rockfall Volume and Hazard Assessment: A Case Study at Southwestern Saudi Arabia," *Egyptian Journal of Remote Sensing and Space Science*, vol. 25, no. 2, pp. 435-443, Elsevier, Aug 2022.
The definitive version is available at https://doi.org/10.1016/j.ejrs.2022.03.010

The Egyptian Journal of Remote Sensing and Space Sciences 25 (2022) 435–443

HOSTED BY

Contents lists available at ScienceDirect

The Egyptian Journal of Remote Sensing and Space Sciences

journal homepage: www.sciencedirect.com

Temporal LiDAR scanning in quantifying cumulative rockfall volume and hazard assessment: A case study at southwestern Saudi Arabia ☆

Abdullah A. Alotaibi [a], Norbert H. Maerz [b], Kenneth J. Boyko [b], Ahmed M. Youssef [a,c], Biswajeet Pradhan [d,e,f,*]

[a] Saudi Geological Survey, Geological Hazards Department, P.O. Box 54141, Jeddah 21514, Saudi Arabia
[b] Missouri University of Science and Technology, Geological Engineering, 1006 Kingshighway, Rolla, MO 65409, USA
[c] Geology Department, Faculty of Science, Sohag University, 82524 Sohag, Egypt
[d] Centre for Advanced Modelling and Geospatial Information Systems (CAMGIS), School of Civil and Environmental Engineering, University of Technology Sydney, NSW 2007, Australia
[e] Center of Excellence for Climate Change Research, King Abdulaziz University, P. O. Box 80234, Jeddah 21589, Saudi Arabia
[f] Earth Observation Center, Institute of Climate Change, Universiti Kebangsaan Malaysia, 43600 UKM Bangi, Selangor, Malaysia

ARTICLE INFO

Article history:
Received 13 September 2021
Revised 3 February 2022
Accepted 16 March 2022

Keywords:
LiDAR
Laser scanning
Rockfall
Remote sensing
GIS
KSA

ABSTRACT

Rockfalls and unstable slopes pose a serious threat to people and property along roads/highways in the southwestern mountainous regions of Saudi Arabia. In this study, the application of terrestrial light detection and ranging (LiDAR) technology was applied aiming to propose a strategy to analyze and accurately depict the detection of rockfall changes, calculation of rockfall volume, and evaluate rockfall hazards along the Habs Road, Jazan Region, Saudi Arabia. A series of temporal LiDAR scans were acquired at three selected sites. Our results show that these three sites have different degrees of hazard due to their geological differences. The mean volume loss of sites A1, A2, and A3 is 327.1, 424.4, and 3.7 L, respectively. Statistical analysis confirms the significance of the influence of site type on rockfall volume, with a probability value of < 0.0105. The rockfall volume and change detection values are then correlated with precipitation, which is a triggering factor. The study also reveals that the use of terrestrial LiDAR could reduce time and effort, increase accessibility, and produce effective solutions. LiDAR could be an indispensable tool for disaster risk assessment, response and recovery process.

1. Introduction

Rockfalls detach from a high rocky area (cliff/slope) due to the influence of gravity (Dunham et al., 2017), exhibiting various motion types such as rolling, bouncing, flying, and sliding, which have immense volumes of up to over 100 m^3. These rockfalls are posing a major hazard and serious risks to lifelines (roads, highways and pipelines) of mountainous areas (Ansari et al., 2014). Rockfall events vary temporally and spatially, making it challenging to predict. To eliminate or reduce rockfall damage to property and save human lives, a proper evaluation of rockfall hazard is necessary. This will help developers to be proactive in planning urban areas. Monitoring of rockfall activity plays a crucial role in predicting hazards and risks (Kenner et al., 2014).

Measuring rockfall volume with conventional direct measurements is inaccurate at best and consists of an approximation of the volume of rock retained in the roadside ditch. The development of new technologies promises many benefits in measuring rockfall quantity (volume) (Williams et al., 2018). LiDAR (laser) scanners are becoming more prevalent because they provide: highly accurate measurements, reach inaccessible locations, and offer greater confidence and repeatability (Farmakis et al., 2020). The use of 3D imagery generated by LiDAR is an advanced method for measuring rockfall volumes due to its capability to provide high vertical and horizontal resolution (van Veen et al., 2017). LiDAR has been used in various studies, such as rock mechanics, to determine the geometry of discontinuities; landslides to quantify rockfall rates and to monitor spatio-temporal changes/deformations with a high level of detail; and for quantifying rockfall hazard models (Wang et al., 2017; Fanos and Pradhan, 2018, 2019; Li et al., 2019; Jiang et al., 2020).

Along the mountainous areas in the southwestern part of KSA, rockfall is considered as a human-induced hazard. The Habs escarpment road is situated in the district of Bani Malek, Jazan region, in the southwestern part of Saudi Arabia, at 17°22′43″N

Peer review under responsibility of National Authority for Remote Sensing and Space Sciences.

* Corresponding author at: Centre for Advanced Modelling and Geospatial Information Systems (CAMGIS), School of Civil and Environmental Engineering, University of Technology Sydney, NSW 2007, Australia.

E-mail addresses: otaibi.aa@sgs.org.sa (A.A. Alotaibi), k.j.boyko@mst.edu (K.J. Boyko), Biswajeet.Pradhan@uts.edu.au (B. Pradhan).

https://doi.org/10.1016/j.ejrs.2022.03.010
1110-9823/

and 43°11′39″E (Fig. 1). The current road serves as an important link road between the scattered small towns and villages and the main coastal highway linking the northern part of KSA with the southern foothills. The road has a length of 14 km, with a very winding route through rugged mountains with rock cuts through different types of rock formations. Since its construction, there has been very little monitoring and maintenance of the road's condition, and no attempt has been made to estimate rockfall rates in a traditional or non-traditional manner. At the same time, rockfall events continue to occur, posing a threat to life and property and disrupting economic activity due to the closed road. In this study, LiDAR technology has been used to perform the followings tasks: (i) to apply change detection and quantify rockfall volumes using temporal LiDAR scanning; (ii) to investigate the effects of different rock cliff/slope characteristics on rockfall volume changes; and (iii) to demonstrate the benefits of using LiDAR technology in rockfall hazard assessment. The application of terrestrial LiDAR is a novel work in Saudi Arabia and could be applied in the construction of 3D perspectives to detect and characterize rockfall activity and rockfall scaling.

2. Review of terrestrial LiDAR application

Laser scanners (LiDAR) are based on time-of-flight measurement between the emitted beam and the reflected pulse from the object and can detect millions of points in a few minutes (Jiang et al., 2020). The time-of-flight of the emitted and returned signals is measured and utilized to calculate the actual distance to the target using equation (1) (Andrew et al., 2012).

$$Distance = \frac{(SpeedofLight * TimeofFlight)}{2} \quad (1)$$

Pradhan and Fanos (2017) indicated that unnecessary data (outliers) generated by the LiDAR errors or multipath beams can be deleted using certain filters and interpolation techniques. Many authors have applied LiDAR imagery to assess and monitor different types of natural processes (Kogut and Pilecka, 2020). Worldwide, terrestrial LiDAR 3D imagery is widely used to assess rockfall hazards along highways and roads (Rammer et al., 2010; Tonini and Abellan, 2014; Carrea et al., 2015). Laser scanning point clouds have been used to automatically extract discontinuities (Vöge et al., 2013) with many advantages over manual methods in which human bias will minimized and the acceleration of results tenfold. The recognition of rockfall source areas and the identification of discontinuities are important concerns in rockfall hazard assessment (Fanos and Pradhan, 2018). Terrestrial and airborne LiDAR scans were also used by Kuhn and Prüfer (2014) to monitor steep, high-elevation sites and deep-seated active landslides by quantifying change and volume detection through temporal scanning methods.

3. Instrument and testing sites

In this study, a LiDAR scanner (ScanStation II®), tripod, tribrach, Cyclone® software, generator, power supply for LiDAR and computer, and Ethernet interconnect cable were used (Fig. 2a). Three sites were selected for this study along Habs Mountain Road (Fig. 2b, c, d). Site (A1), paleochannel materials (debris flow materials), is located at 17°22′38″N and 43°12′11″E and has a width of 23 m and a height of 24 m (Fig. 2b). This site is characterized by two sections, the lower of which is a stable, nearly vertical hard rock wall approximately 2.5 m high and the upper of which has a low angle containing boulders in matrix deposits (gullies) that lie above the rock outcrop and extend to the top of the outcrop. Site (A2), a bedrock layer composed of small to medium-sized basalt blocks, is located at 17°22′47″N and 43°11′56″E. It is 19 m wide and 19.5 m high (Fig. 2c). It is characterized by in situ fractured boulders in the top portion and regolith, covering the bottom section. Site (A3), bedrock, which is affected by different joint sets, is located at 17°22′43″N and 43°11′40″E with 20.6 m width and 23.5 m height (Fig. 2d).

4. Data collection and processing

4.1. Data collection

The starting and ending points of each area were marked with paint, measuring its distance and height. The scan resolution was chosen according to the respective site dimensions (width and height) and the processing limits of the software, i.e. the resolution

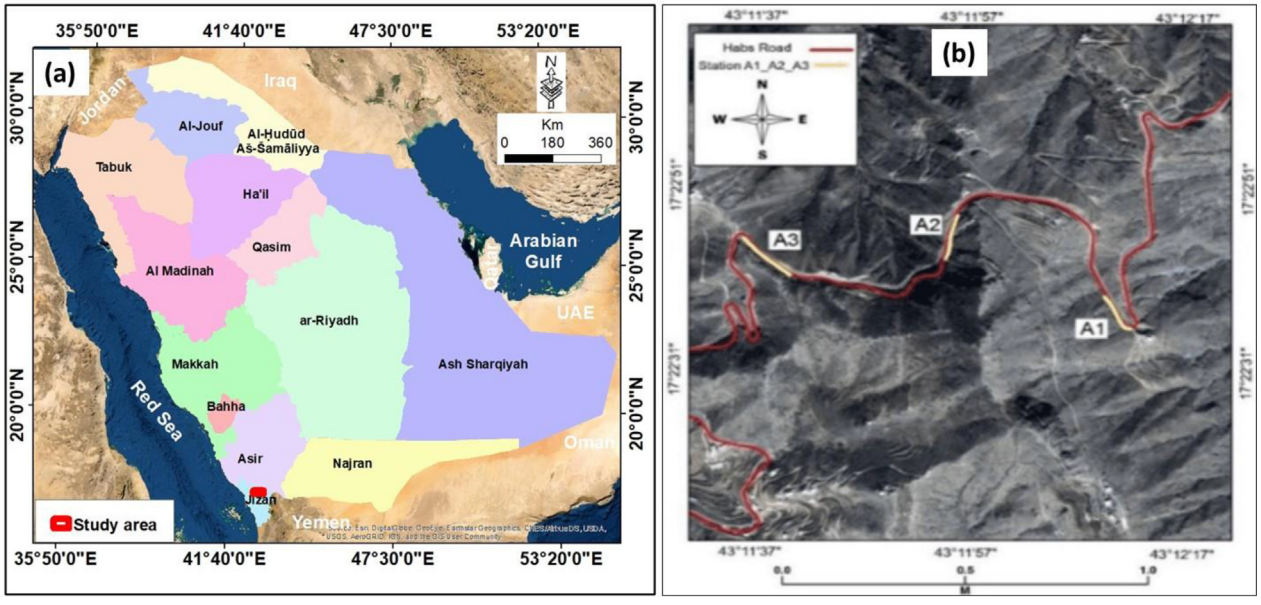

Fig. 1. (a) Location of the study area in KSA; and (b) Location of the three sites selected for the study at Habs Mountain Road.

Fig. 2. (a) The equipment used for data collection, (b), (c), and (d) sites A1, A2, and A3, respectively.

was adjusted to complete the full scan in the time available for fieldwork. To identify the exact location of the scanner, solid metal poles were used at sites A2 and A3, and site A1 was marked with red spray paint. This technique was applied to ensure that all measurements taken at different times were of high precision. The tripod and ScanStation II were leveled, although the registration procedure developed for this project did not require the scanner to be leveled. Several steps are performed in the following order: 1) determine the LiDAR location; 2) conduct the LiDAR setting; and 3) measure the distance between the scanner location and the object. Table 1 shows the data collected at the three sites. The final step of data collection was to scan objects at different times from the same scanner location.

4.2. LIDAR data processing

In its simplest form, the data acquired by the LiDAR device are distance values in directions XYZ coordinates and beam intensities (I) reflected from the target under study (Fig. 3a). The result of the LiDAR survey is in the form of a point cloud, which is displayed in a red, green, and blue (RGB) color image format using a tool built into the LiDAR scanner (Fig. 3b). Sometimes, this data is referred to as a dense digital surface model (DDSM). Various file formats can be generated from the LiDAR point cloud data using a specially designed software. In the current study, ASCII point file format (.pts) was used in which each point is represented as a single line (Fig. 4). A software was developed in a popular programming language (C++) by Boyko (2012) was used to transfer the original point cloud data to a depth image format (.pts file format) with a dimension of 4300 cells in raw and 3400 cells in columns to calculate the rockfall volume. These data were projected onto a spherical surface. Each cell in the generated model considers a single point in the point cloud data. It includes the range, intensity and RGB color values which are stored in a file in a binary format for effective processing.

The processing of the data was done in a series of seven main steps (Fig. 5). The preliminary goal of the action is to obtain a clean file, followed by georeferencing of the scans and calculation of the volume of rockfall. These seven steps were conducted using particular software, which was developed by Boyko (2012) with the exception of cyclone: these steps are:

A) Cyclone software: used to manage the LiDAR scanner instrument throughout data acquisition procedure and to convert the data for further processing.
B) FindMinMax: it finds the XYZ minimum and maximum values for the point cloud area in the vertical and horizontal directions to limiting the processing window to the point cloud area of the raw data file (.pts).
C) Load: a raster format file (grid/mesh) with the same original scan resolution is generated from the raw scan data and the empty pixels will be filled using the interpolation technique.
D) Register: it is the essential key element, in which all scan images are registered with great accuracy (Fig. 6). To complete the registration process, four conjugate control points in each scan image must be identified by the operator. This essentially converts the images from LIDAR to the base-datum coordinates. The residual errors of the transformation are calculated, and the 3D residuals are an indicator of the general agreement between two scan coordinate systems.

Table 1
Scanning parameters used in the current study.

Station Number	Scan resolution (mm)	Probe distance (mm)	Height (m)	Length (m)	Number of scan points
A1	8	14,384	24	23	2,641,944
A2	6	15,341	19.5	19.2	9,500,000
A3	10	12,477	23.4	20.6	5,011,652

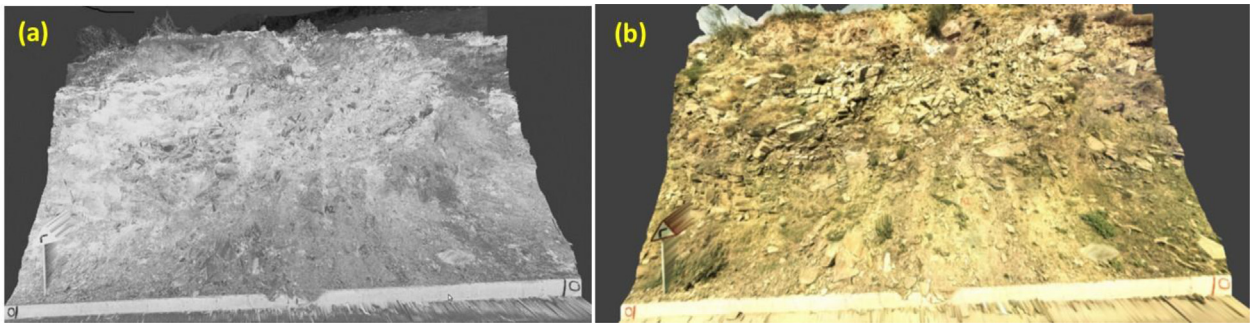

Fig. 3. (a) Intensity image of site A2 obtained with the ScanStation 2 scanner. (b) RGB image created with the ScanStation II from site A2.

X	Y	Z	I	R	G	B
-6.866426	8.429932	-2.176701	-808	153	152	113
-6.902613	8.474385	-2.179079	-771	154	154	111
-6.941738	8.522446	-2.182240	-755	136	137	93
-7.093397	8.708940	-2.220519	-562	137	137	94
-7.102941	8.720685	-2.213958	-462	127	128	86
-7.107734	8.726596	-2.205848	-540	123	121	86
-7.118383	8.739698	-2.199489	-731	119	118	83

Fig. 4. Shows the main extracted data from (.pts) files.

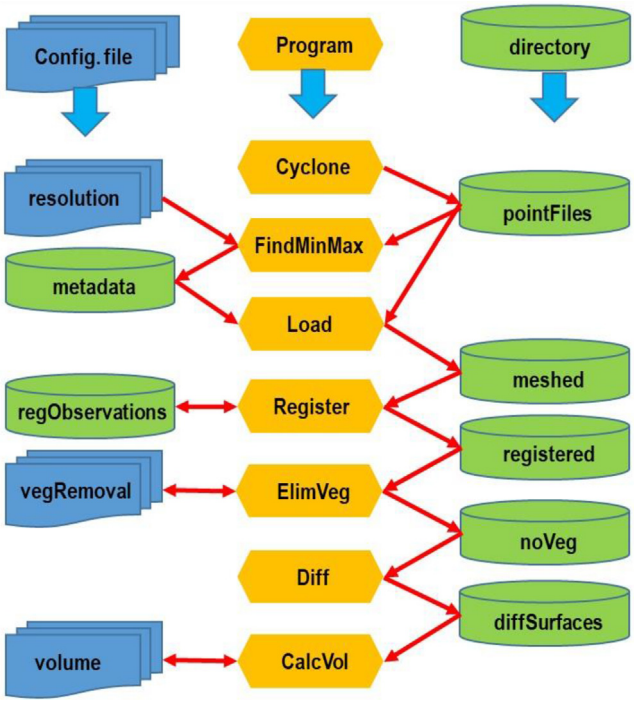

Fig. 5. Flow chart of data processing steps.

It was found that the overall root-mean-square-error (RMSE) ranges from 1.3 mm (good agreement) to 11.4 mm (poor agreement).

E) ElimVeg: it detects and removes spikes in data generated by vegetation cover (grass and trees) using special filters (Fig. 7).

F) Diff: in this step, subtraction techniques were used for change detection and comparison between successive scans to generate a difference surface image based on equations (2 and 3), detecting changes (positive and negative) and no changes when the difference was zero. In the current study, the threshold of 0 L was detected as no change. Changes were calculated in liters as it was suggested by Kassebaum (2012). To evaluate the overall difference between two epochs, changes between the different scans were detected using a pixel-to-pixel algorithm. It provides rockfall blocks as negative values (loss) below the threshold and accumulated material as positive values (gain) above the threshold.

$$d_{i,j}chnage(\pm) = R_{i,j} - A_{i,j} \quad (2)$$

$$d_{i,j}nochnage = R_{i,j} - A_{i,j} = 0 \quad (3)$$

where, dij is pixels in the difference image, Rij is the pixels in the reference scan image, Aij is the number of pixels in the analyzed scan image.

G) CalcVol: calculating the volume of falling rocks is the final step in these procedures. However, several potential errors should be evaluated prior to this step, including artifacts, incomplete elimination of vegetation, discrepancies between site and date of scan, scanner accuracy, and configuration of scanner elements. Note, the LiDAR instrument's exact location and the registration process must be performed with care.

5. Results and discussion

In this work, a comprehensive 3D slope stability analysis was done using LiDAR. The investigated areas indicated that some sites can hold high risk and require mitigation measures. The change detection works focus on deformation analysis for designated objects. Three study areas were scanned between June 28/2013 and September 12/2013. In each case, six scans were made during this period to produce a surface map of the cliff face. The first scan was processed, and the second through sixth scans were cropped to the coordinate system of the first scan and registered with the scans. Comparison was performed by the subtraction of a resampled set of the data as shown in Figs. 8 and 9. The technique was applied to the whole scene.

The analysis was compared with respect to the reference, i.e., the first scan image acquired on June 28. The detection threshold was set to 0 (no difference). Due to space constraints, we do not extend this comparison to multiple scans and note that extending this approach is quite straightforward. Changes in each step between the two temporal scenes are identified. The level of detail that can be detected in different domains is shown in Figs. 8 and 9. These change detections are represented in loss (negative) and gain (positive) values. Considering the very different views from which the two scenes were taken, the ability to detect changes of differ-

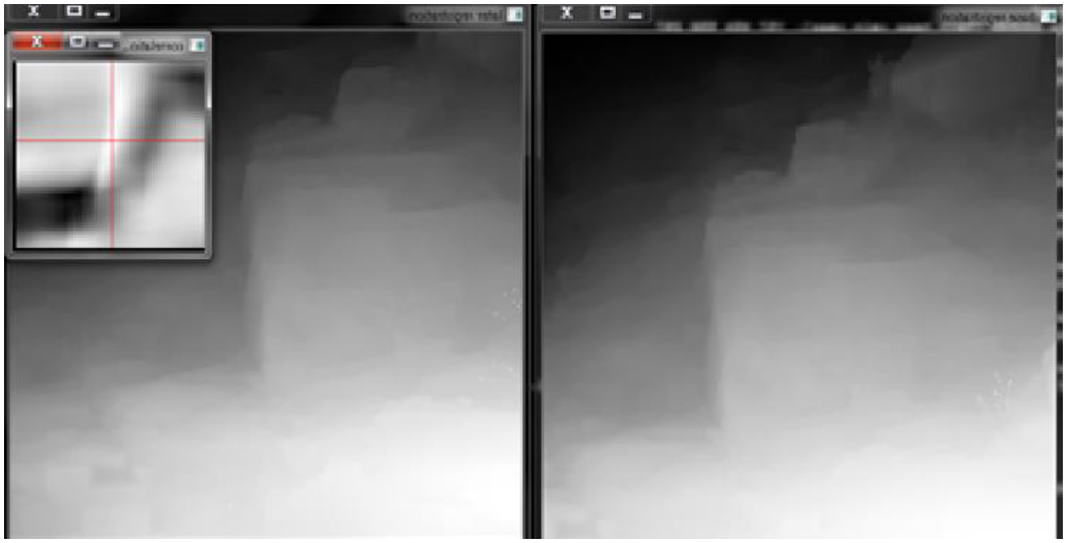

Fig. 6. Images showing the registration process. Note that the small box indicates how well the two points match.

Fig. 7. The vegetation cover before removal in the right image and after removal in the left image.

ent magnitudes and within a cluttered natural environment is very good. Since the comparison is done by image subtraction, the detection of differences is almost instantaneous and requires mainly the transformation of the analyzed scan to the reference scene and, when the whole change is sought, the application of the same transformation is in reverse order. The difference between each of the second through sixth scans and the first surface map was calculated, resulting in a cumulative difference map for each successive scan.

The results for sites A1, A2, and A3 indicated that the difference between the rock surfaces from scan 1 and scans 2, 3, 4, 5, and 6 is quantified in Fig. 8, which shows five difference maps. Each white area represents a single block (boulder) or group of blocks (boulders) that have fallen out of their previous position. Where there was a net volume gain on the difference image, the area was highlighted in red. There were very few and only small red zones, which could represent small blocks that returned to their position after falling from above, or could be small registration errors during scanning. Fig. 9 shows the cumulative volume of lost and recovered rock in liters. At Site A1, registration errors in scans 6–29 and 09–12 resulted in less volume lost than in the previous scan, which is not necessarily the case with a cumulative measurement. This registration error does not occur at sites A2 and A3, where the cumulative results show a good pattern of cumulative rock loss at the rock face, except for the period between 7/2 and 8/23, when very little rock was lost.

In the scan of site A1 from 6 to 28 and 6–29 image (Fig. 8), some lost materials have appeared on the upper right side of the image. This is most likely an error due to poor registration and tilting of one scan relative to the other. Another factor that can cause errors in the registration of recovered or lost material is parallax error, which is caused by the shift of the LiDAR instrument between suc-

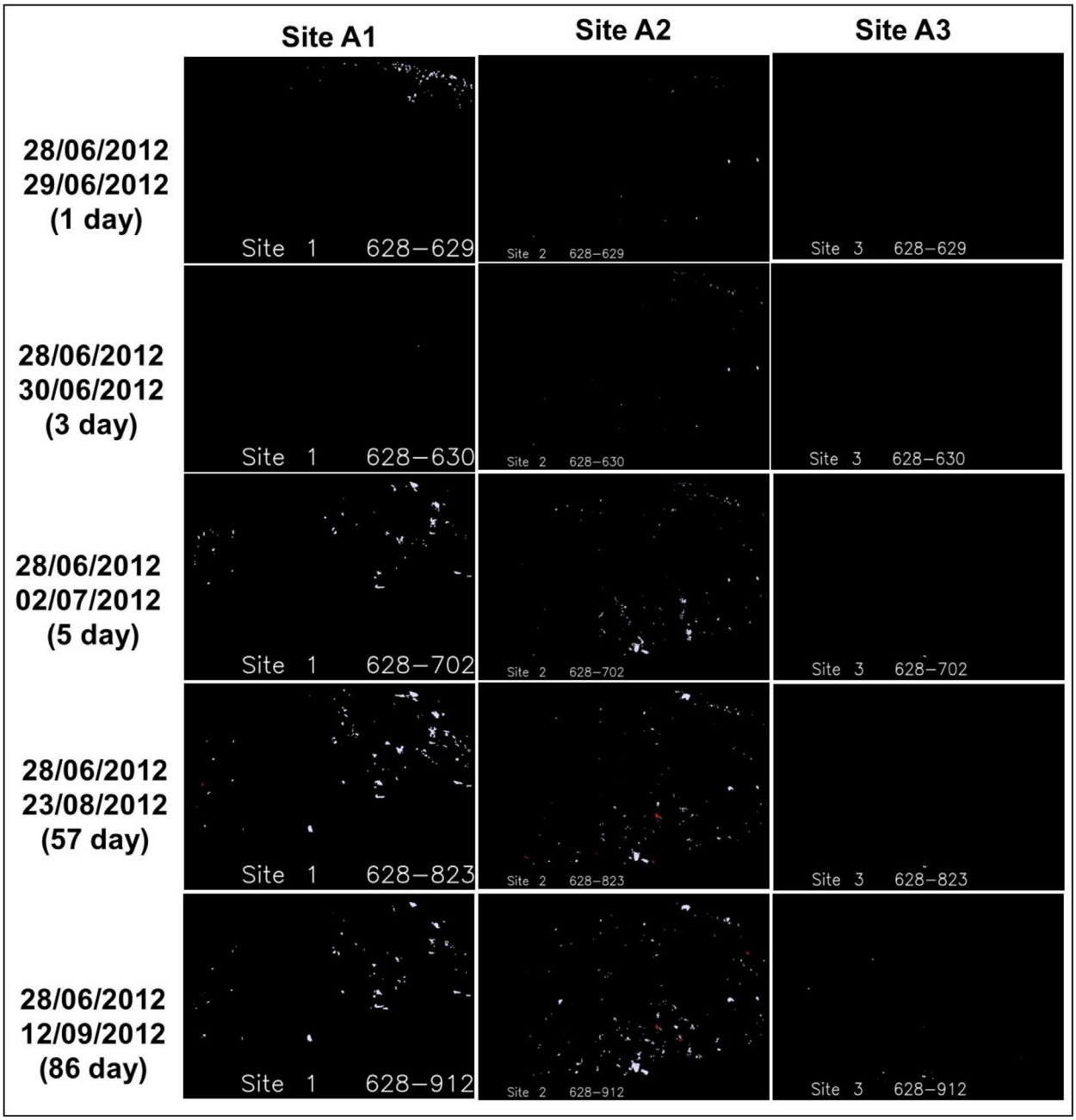

Fig. 8. Difference scanning results for sites A1, A2, and A3. White and red areas represent rock loss and gain respectively based on difference scans between the initial scan (6/28/2013) and scans taken 6/29/2013, 6/30/2013, 7/02/2013, and 8/23/2013, and 9/12/2013 for all thre sites. (For interpretation of the references to color in this figure legend, the reader is referred to the web version of this article.)

cessive scans. Analysis of the data shows that most of this shift occurred in the x-direction. While it is possible that other factors may contribute to an increase if there has been a prior loss of material, such as material being washed or slurried into voids previously created by rockfall, this is likely not the case here. This would have been the result of runoff, precipitation, seismic activity, or even animal-triggered falls. Although earthquakes are common in the study area, there were none during this period.

Field observations indicate that the topmost portion of site A1 is probably a paleo-filled channel (block-in-matrix deposits), with large, truncated blocks occupying the bottom portion of the filled channel and the finer, weaker sediments occupying the top portion (Fig. 2b). The lower right part of the site consists of trimmed bedrock. Thus, the lost material is preferentially from the less stable upper and left part of the site, as shown in Fig. 8. The last scan (09-12) showed a decrease in the calculated volume compared to the previous scans (Fig. 9), which may be as a result of the previously mentioned errors.

Site A2 consists of small to medium-sized basalt blocks (Fig. 2c). These blocks have sharp edges, indicating less susceptibility to weathering processes or recent fractures. Site (A2) showed a constant increase in lost material from 150 L to 588 L (Fig. 9). The increase in recovered material could be attributed to void flushing by unconsolidated material or by rock falling into the voids from above.

Site A3: This site is different from the other two sites (A1 and A2). It consists of hard metamorphic rocks with fewer fractures, mainly metasedimentary (Fig. 2d), and consequently had much

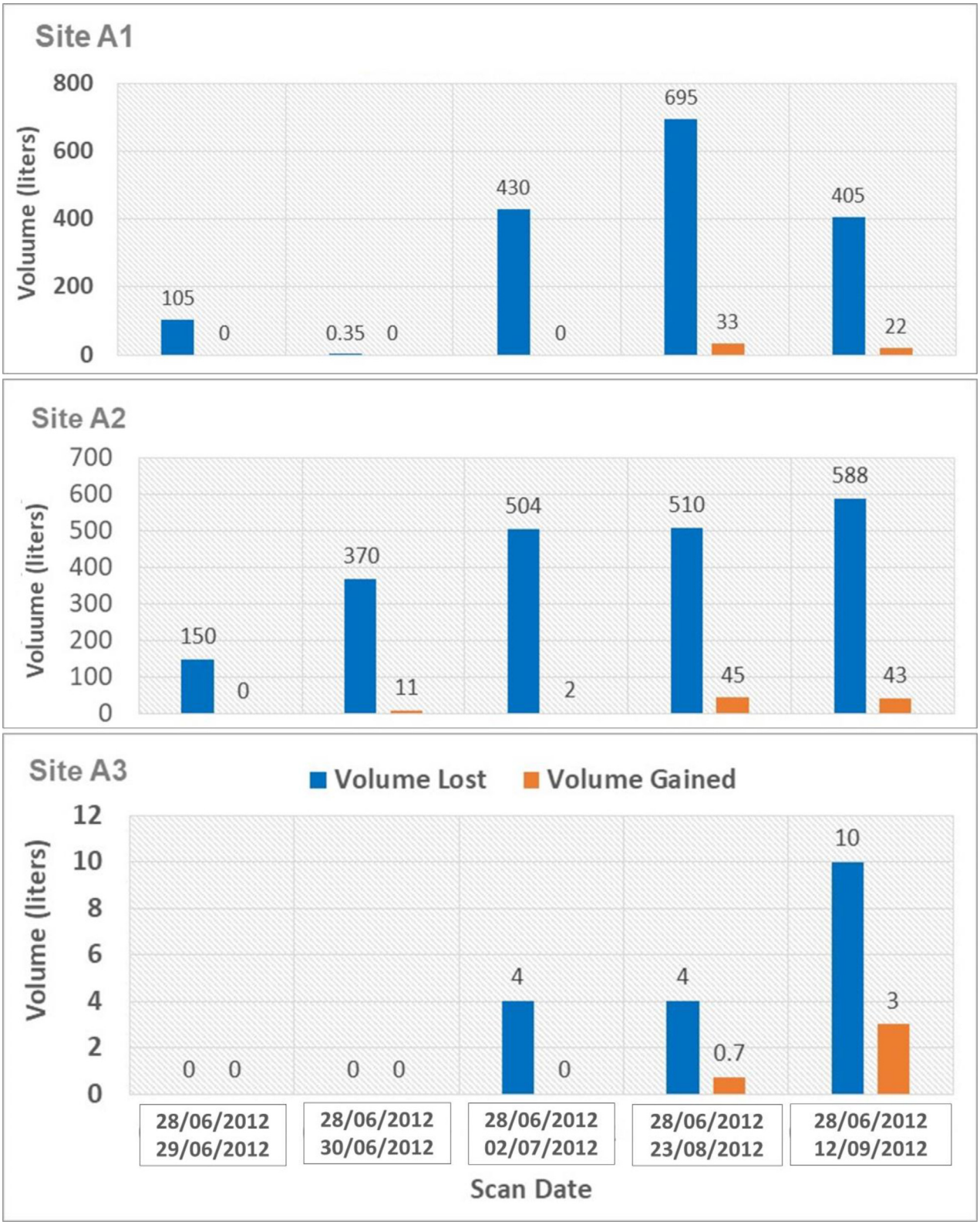

Fig. 9. Change in rock volume (loss and gain) at site A1, A2, and A3. Each bar represents the cumulative volume through sixth scans compared to the first scan.

smaller amounts of lost rock. Scans showed no change in lost volume on the second and third images (Figs. 8 and 9). A slight increase in lost material was noted on the fourth through sixth scans, while the significant increase in lost material occurred on the last scan.

In addition, a statistical analysis was performed to compare the fallen rocks of the three sites A1, A2 and A3 (Table 2). The statistical analysis of the data showed that the highest mean value is associated with site A2, followed by site A1, and the lowest mean value is for site A3. In contrast, the standard deviation is highest for site

Table 2
Descriptive statistics and one-way ANOVA of the three sites.

Descriptive statistics				One-way ANOVA			
Sites	A1	A2	A3		Between groups	Within Groups	Total
Minimum	0.35	150	0	**Sum of Squares**	485297.7	426851.6	912149.3
Maximum	695	588	10	**DF**	2	12	14
Median	405	504	4	**Mean Square**	242,649	35,571	
Mean	327.1	424.4	3.7	**F Ratio**	6.821		
Standard deviation	277.5	172.3	4.1	Significant	0.0105		

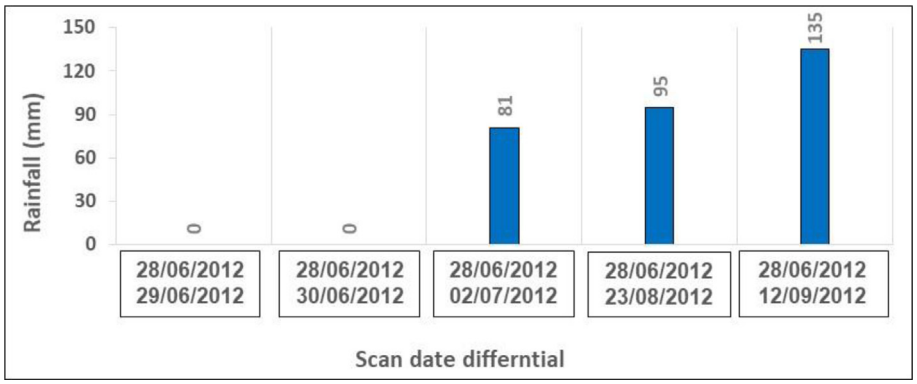

Fig. 10. Precipitation data is cumulative since the first scan.

A1, followed by site A2, and the lowest value is for site A3. The results of the calculations performed to determine the significance of the effect of site type on lost volume are shown in Table 2. The results of the statistical analysis confirm that the sites (A1, A2 and A3) are significantly different in terms of the volume of rockfall lost (p-value < 0.0105). Accordingly, they have a significant influence on the values obtained for the tested parameter, because the p-value was lower than the assumed significance level (α = 0.05). This statistical variability in the parameters of the statistical analysis is due to the different physical and geotechnical properties of the materials at each site.

Finally, precipitation data that have been collected from nearest rain gauge station were analyzed to create a correlation between rockfall changes with rainfall values (Fig. 10). Results show that by increasing the cumulative rainfall values, rockfall increased. Our results are in agreement with various studies, which indicated that there is a strong correlation between precipitation intensity and the triggering of landslides (e.g., rockfalls and debris flows) (Bel et al., 2017; Roccati et al., 2020). In addition, managing rockfall risks have been done by using terrestrial laser scanner and provide so accurate data that could be a help in designing detailed mitigation measures (Kromer et al., 2017).

According to this proposed methodology, including the use of LiDAR in rockfall modeling and identifying the rockfall trajectories and final deposition areas. Using the 3D LiDAR model has the capability to understand the relationship between the falling rocks and detailed topography. Also, it will help in identifying the optimum mitigation measures that could help planners and decision makers to be proactive.

6. Conclusions

This study has illustrated the feasibility and effectiveness of using LiDAR in change detection, volume calculation, and rockfall hazard analysis. In the current study, there was no historical rockfall volume estimate that could be used as a reference to compare the results. A number of limitations have been discussed in various studies associated with traditional rockfall surveys, including safety issues, terrain inaccessibility, and human error (particularly error associated with measuring irregular blocks located in uneven trenches). In addition, it is difficult to cover relatively large areas, requiring significant manpower, cost, and logistics. The application of LiDAR technique offers more advantages than conventional methods. Acquiring dense 3D data of a terrain with high speed and accuracy and significantly efficient processing could help to better quantify the main factors controlling slope instabilities, using spatial scales (volumes from tens of cubic centimeters to millions of cubic meters) and temporal scales (from days to years). Statistical analysis of the data showed that site A1 has high variability, followed by site A2, and the lowest variability is associated with site A3. The results were verified by a one-way ANOVA test, where the three sites differ significantly in terms of lost rockfall volume due to their different physical and geotechnical characteristics (p-value < 0.0105). The current study considers a number of challenges: Voids could be created along steep slopes/road cuts by falling rocks. Later, these voids could be refilled by falling materials. Otherwise, these boulders reach a stable condition (as they rest on the ground surface. The main conclusions from this study are as follows: (1) the proposed technique can be applied with great accuracy to capture 3D images of distant rock slopes and inaccessible cliffs. (2) The accuracy of the model of rockfall change detection and volume calculation depends on accurate registration step. (3) The results show that the assessment of rockfall hazard is essential for engineering measures.

Declaration of Competing Interest

The authors declare that they have no known competing financial interests or personal relationships that could have appeared to influence the work reported in this paper.

Acknowledgments

We thank Saudi Geological Survey for funding this study. We also thank the Rock Mechanics and Explosives Research Centre at MST for software development support.

References

Andrew, R., Arndt, B., Turner, K.A., 2012. Instrumentation and Monitoring Technology, Rockfall characterization and control. Transportation Research Board of the National Academies Press, Washington, D.C., pp. 212–276.

Ansari, M.K., Ahmad, M., Singh, T.N., 2014. Rockfall risk assessment for pilgrims along the circumambulatory pathway, Saptashrungi Gad Temple, Vani, Nashik Maharashtra, India. Geomat. Nat. Hazards Risk 5 (1), 81–92.

Bel, C., Liébault, F., Navratil, O., Eckert, N., Bellot, H., Fontaine, F., Laigle, D., 2017. Rainfall control of debris-flow triggering in the Réal Torrent, Southern French Prealps. Geomorphology 291, 17–32.

Carrea, D., Abellan, A., Derron, M.-H., Jaboyedoff, M., 2015. Automatic Rockfalls Volume Estimation Based on Terrestrial Laser Scanning Data. In: Lollino, G., Giordan, D., Crosta, G.B., Corominas, J., Azzam, R., Wasowski, J., Sciarra, N. (Eds.), Engineering Geology for Society and Territory - Volume 2. Springer International Publishing, Cham, pp. 425–428. https://doi.org/10.1007/978-3-319-09057-3_68.

Dunham, L., Wartman, J., Olsen, M.J., O'Banion, M., Cunningham, K., 2017. Rockfall Activity Index (RAI): A lidar-derived, morphology-based method for hazard assessment. Eng. Geol. 221, 184–192.

Fanos, A.M., Pradhan, B., 2019. A novel rockfall hazard assessment using laser scanning data and 3D modelling in GIS. Catena 172, 435–450. https://doi.org/10.1016/j.catena.2018.09.012.

Fanos, A.M., Pradhan, B., 2018. Laser Scanning Systems and Techniques in Rockfall Source Identification and Risk Assessment: A Critical Review. Earth Syst. Environ. 2 (2), 163–182. https://doi.org/10.1007/s41748-018-0046-x.

Farmakis, I., Marinos, V., Papathanassiou, G., Karantanellis, E., 2020. Karantanellis E (2020) Automated 3D Jointed Rock Mass Structural Analysis and Characterization Using LiDAR Terrestrial Laser Scanner for Rockfall Susceptibility Assessment: Perissa Area Case (Santorini). Geotech. Geol. Eng. 38 (3), 3007–3024.

Jiang, C., Chen, Y., Tian, W., Feng, Z., Li, W., Zhou, C., Shao, H., Puttonen, E., Hyyppä, J., 2020. A practical method utilizing multi-spectral LiDAR to aid points cloud matching in SLAM. Satell. Navig. 1 (1). https://doi.org/10.1186/s43020-020-00029-5.

Kassebaum, T.J., 2012. Using LiDAR as a monitoring device to calculate volume of rockfall over time. Masters Theses 5303 https://scholarsmine.mst.edu/masters_theses/5303.

Kenner, R., Bühler, Y., Delaloye, R., Ginzler, C., Phillips, M., 2014. Monitoring of high alpine mass movements combining laser scanning with digital airborne photogrammetry. Geomorphology 206, 492–504. https://doi.org/10.1016/j.geomorph.2013.10.020.

Kogut, J.P., Pilecka, E., 2020. Application of the terrestrial laser scanner in the monitoring of earth structures. Open Geosci. 12 (1), 503–517. https://doi.org/10.1515/geo-2020-0033.

Kromer, R., Lato, M., Hutchinson, D.J., Gauthier, D., Edwards, T., 2017. Managing rockfall risk through baseline monitoring of precursors using a terrestrial laser scanner. Can. Geotech. J. 54 (7), 953–967. https://doi.org/10.1139/cgj-2016-0178.

Kuhn, D., Prüfer, S., 2014. Coastal cliff monitoring and analysis of mass wasting processes with the application of terrestrial laser scanning: A case study of Rügen, Germany. Geomorphology 213, 153–165.

Li, H.-b., Li, X.-w., Li, W.-z., Zhang, S.-l., Zhou, J.-w., 2019. Quantitative assessment for the rockfall hazard in a post-earthquake high rock slope using terrestrial laser scanning. Eng. Geol. 248, 1–13. https://doi.org/10.1016/j.enggeo.2018.11.003.

Rammer, W., Brauner, M., Dorren, L., Berger, F., Lexer, M., 2010. Evaluation of a 3-D rockfall module within a forest patch model. Nat. Hazards Earth Syst. Sci. 10 (4), 699–711.

Roccati, A., Paliaga, G., Luino, F., Faccini, F., Turconi, L., 2020. Rainfall Threshold for Shallow Landslides Initiation and Analysis of Long-Term Rainfall Trends in a Mediterranean Area. Atmosphere 11, 1367. https://doi.org/10.3390/atmos11121367.

Tonini, M., Abellan, A., 2014. Rockfall detection from LiDAR point clouds: a clustering approach using R. J. Spat. Inf. Sci. 8, 95–110. https://doi.org/10.5311/JOSIS.2014.8.123.

van Veen, M., Hutchinson, D.J., Kromer, R., Lato, M., Edwards, T., 2017. Effects of sampling interval on the frequency-magnitude relationship of rockfalls detected from terrestrial laser scanning using semi-automated methods. Landslides 14 (5), 1579–1592.

Vöge, M., Lato, M.J., Diederichs, M.S., 2013. Automated rockmass discontinuity mapping from 3-dimensional surface data. Eng. Geol. 164, 155–162.

Wang, M., Liu, K., Yang, G., Xie, J., 2017. Three-dimensional slope stability analysis using laser scanning and numerical simulation. Geomat. Nat. Hazards Risk 8 (2), 997–1011. https://doi.org/10.1080/19475705.2017.1290696.

Williams, J.G., Rosser, N.J., Hardy, R.J., Brain, M.J., Afana, A.A., 2018. Optimising 4D Approaches to Surface Change Detection: Improving understanding of rockfall magnitude–frequency. Earth Surf. Dyn. 6, 101–119. https://doi.org/10.5194/esurf-2017-43.